Dynamics in Bridge-Rich Thermoresponsive Micellar Networks

Benedetta Rosi,[*,†,‖] R. Biehl,[†] J. Allgaier,[†] K. Schwärzer,[†] W. Pyckhout-Hintzen,[†] O. Czakkel,[‡] S. Prevost,[‡] N. R. de Souza,[¶] O. Holderer,[§] S. Förster,[†] and M. Kruteva[†]

†*Jülich Centre for Neutron Science (JCNS), Forschungszentrum Jülich GmbH, 52425 Jülich, Germany*

‡*Institut Laue-Langevin (ILL), 71 Av. des Martyrs, 38000 Grenoble, France*

¶*Australian Nuclear Science and Technology Organisation (ANSTO), New Illawarra Road, Lucas Heights, NSW 2234, Australia*

§*Jülich Centre for Neutron Science at MLZ, Forschungszentrum Jülich GmbH, Lichtenbergstraße 1, 85748 Garching, Germany*

‖*Present address: European Spallation Source ERIC, 224 84 Lund, Skåne County, Sweden*

E-mail: benedetta.rosi@ess.eu

Abstract

Block copolymers containing thermoresponsive poly-N-isopropyl acrylamide (PNIPAM) and a persistently hydrophobic block, like polystyrene (PS), form micellar gels in water when triblock (PS-PNIPAM-PS) are added as they interconnect micelles. Neutron scattering methods utilizing specific deuteration strategies allow to address the structure and dynamics with a focus on PNIPAM bridging blocks. Triblocks increase the mechanical stability depending on the number of bridges formed. Small-angle neutron scattering (SANS) allows us to observe the arrangement of triblocks around the

micellar core, and confirms that a large number of blocks is in bridging configuration. The dynamics of the bridges is Zimm-like, with significant changes due to the fixed ends but presents internal friction like free PNIPAM. A characteristic modulation in the dynamics related to the geometrical arrangement is found. Side chains are mobile but strongly constrained by a much slower backbone. The theoretical approach derived herein can serve as a framework for describing other systems in which polymeric junctions play a significant role.

Introduction

Responsive hydrogels are popular smart materials, consisting of 3-dimensional cross-linked networks with the ability to adsorb and retain a large amount of water. Due to their unique properties, including chemical malleability, flexibility, tunability, and biocompatibility they are currently one of the most attractive materials in fields as biomedical tissue engineering and advanced drug delivery.[1–3] The responsive nature is imparted by the presence of stimuli-responsive "switching" polymer moieties[4] allowing the gel to undergo sharp, reversible changes in response to variation of external control parameters (e.g. temperature).[5,6] Among them, poly-N-isopropyl acrylamide (PNIPAM) is probably the most popular polymer due to its well-known thermoresponsive behavior, with a lower critical solution temperature (LCST) in water close to physiological temperatures (LCST $\approx 32^{\circ}$C). The thermoresponsive character of PNIPAM-based systems make them attractive for theoretical and applied studies.[7–11]

The key functional properties of hydrogels rely on their cross-linked structure. Two main routes are currently exploited for cross-link formation, namely, chemical and physical cross-linking. In the former, the network is realized thanks to covalent cross-linking between hydrophilic moieties, while in the latter the connection is established by noncovalent forces. An example is that of block copolymer micellar gels, that demonstrate both the cohesive strength of solids and the diffusive transport characteristics of liquids, and are therefore sub-

ject of theoretical and technological interest.[12–15] In this sense, kinetically "frozen" micelles, where the exchange of polymer chains becomes extremely slow, can be considered as an intermediate system between chemical and physical crosslinked networks.[16] An exemplary case is that of polystyrene (PS) and PNIPAM diblock[17–19] and PS-PNIPAM-PS triblock copolymers.[20–25] While PS-PNIPAM diblock copolymers assume a "star-like" configuration, with the PNIPAM block having one end grafted to the PS core and the other reaching out into the solvent, in PS-PNIPAM-PS triblocks the PNIPAM block can fold in a loop, with both the PS end blocks sticking into the same micellar core. However, such a configuration is entropically unfavorable, and having one of the two PS blocks sticking out of the original core is energetically possible. Such a free PS block can connect to a neighboring core, acting as a bridge. At sufficiently high concentrations, multiple bridges create a "frozen" network of interconnected micelles,[7,22] with higher mechanical stability compared to diblock copolymer micellar systems.

The control of mechanical properties of the hydrogel and the solute diffusion throughout the network are two crucial aspects in numerous applications. Determining the mechanical response of the network as a function of local properties, such as polymer architecture, as well as the response to temperature variation, is critical e.g. in tissue engineering and soft robotics.[26,27] At the same time, connecting mechanical stability to local mobility is important to quantify transport properties within the gel, since the arrangement and flexibility of the chains in the network have influence on the diffusion of water and of macromolecules (nanoparticles, drugs).[28–30] More in general, addressing questions related to microscopic network structure and dynamics might aid in improving the performances of other systems where the connectivity provided by polymer strands plays a crucial role, e.g. for determining mechanical response as in the case of nanoparticles in polymer nanocomposites.[31] Surprisingly few studies have directly approached this subject.

In this work, we investigated the mechanical properties of model block copolymer micellar gels and connected them to their microscopic structure and dynamics. Two main structural

parameters have been considered, namely, role of PNIPAM block size and architecture. The first issue has been addressed by comparing PS-PNIPAM diblock copolymers with fixed PS block and variable PNIPAM block length, namely, "short" and "long" PS-PNIPAM diblocks (≈4:1 and ≈15:1 of PNIPAM:PS size ratio respectively). The role of architecture have been investigated by comparing PS-PNIPAM diblock and PS-PNIPAM-PS triblock (PNIPAM:PS size ratio ≈15:1) copolymers. A particular focus has been given to the role of triblocks due to their possibility to form junctions. To this purpose, we combined the use of neutron scattering techniques (small-angle neutron scattering for the structure, neutron spin echo and neutron backscattering for the dynamics) with specific deuteration strategies to better isolate the contribution from the PNIPAM block, by matching the PS core to the D_2O solvent. In addition, we systematically investigated the relation between increased connectivity and relative amount of triblocks, by studying diblock/triblock blends where the scattering length density of the diblock has been fully matched to the solvent, to isolate the triblock contribution. For the first time we developed a comprehensive model that describes both the structure and dynamics at the microscopic scale from segmental to residue level, across the LCST. Interestingly, from the analysis it emerges that the dynamics of the network is largely described by that of a PNIPAM chain in solution.

Materials and Methods

Polymer synthesis

In Table 1, we provide the list of polymers investigated in this study, together with their molecular weight M_n and polydispersity PDI (M_w/M_n). All details related to their synthesis are reported in the Supporting Information.

Table 1: List of polymers synthesised for this work. M_n and PDI are the number average molecular masses and polydispersity indices (M_w/M_n) of the final polymer products. For the block copolymers, the molecular weight of the PNIPAM block is also reported.

Polymer	M_n **[kg/mol]**	M_n^{PNIPAM} **[kg/mol]**	**PDI**
PNIPAM10	14.0		1.03
PNIPAM40	39.8		1.06
PNIPAM70	73.2		1.09
dPS-RAFT2	2.6		1.05
hPS-RAFT2	2.2		1.06
dPS-RAFT3	4.4		1.16
hPS-RAFT3	4.0		1.18
dPS-hPNIPAM-S	11.0	8.4	1.03
dPS-h,dPNIPAM-S	11.5	8.9	1.03
hPS-hPNIPAM-S	11.0	8.8	1.07
dPS-hPNIPAM-L	27.8	25.2	1.11
dPS-hPNIPAM-dPS	72.6	68.2	1.18
hPS-hPNIPAM-hPS	43.0	39.0	1.09

Micelle samples preparation

Polymers were dissolved in acetone at a concentration of 1 wt%. Acetone is a good solvent for both the PS and PNIPAM block. Although organic solvents have in general the effect of reducing the LCST in PNIPAM/water mixtures, the addition of acetone causes only a relatively small decrease of the LCST[32] and therefore the PNIPAM block can be maintained in its soluble state during the overall procedure of micelle formation. Water has been added drop wise to the polymer/acetone solution using a syringe pump ($\approx$ 2 mL/min), while the solution was stirred in an ice water bath until a 90/10 water/acetone w/w ratio was reached ($\approx$ 0.1 wt% polymer). A small aliquot was taken to asses the hydrodynamic radius R_H and the low concentration diffusion coefficient D_0 of the micelles by dynamic light scattering (DLS) (Malvern, Zetasizer Nano ZS). The solvent was removed by rotary evaporation and subsequently by high vacuum, until a dry thin film was obtained. The final samples were obtained by adding water to the dry material and allowed to equilibrate for several days. For the diblock/triblock blends, appropriate amounts of each micellar solutions (0.1 polymer wt%) were mixed, with the following relative weight fraction: 20% short diblock, 80% triblock (20% di – 80% tri), 50% short diblock, 50% triblock (50% di – 50% tri), 80% short diblock, 20% triblock (80% di – 20% tri), 90% short diblock, 10% triblock (90% di – 10% tri). The mixed solutions were subsequently subjected to rotary evaporation and high vacuum until

reaching the dry state.

Methods

Rheology

Rheological measurements were performed using a ARES (Rheometric Scientific) setup. A standard 25 mm plate configuration has been used. Oscillatory strain sweep tests have been conducted with a oscillation speed ω of $\omega = 1$ rad/sec. Frequency sweep tests have been conducted at a 5% strain amplitude in a frequency range between $\omega = 1$ rad/s and $\omega = 100$ rad/s. The polymer concentration for all samples was fixed to 10 wt%. Measurements on all samples have been performed at room temperature. The samples were put in stainless steel cups with cover to minimise water evaporation effects. A reference triblock sample was also measured under controlled temperature conditions, namely at T=25°C, T=33°C and 39°C. The temperature was controlled by gas stream. To minimize evaporation effects, the test under controlled temperature condition was performed by covering the exposed sample interface with a low viscosity oil.

Small-angle neutron scattering (SANS)

Small-angle neutron scattering (SANS) measurements were performed at the D33 beamline at the Institut Laue-Langevin (ILL).[33,34] The instrument was used in the monochromatic mode with an incident wavelength of $\lambda = 0.462$ nm ($\Delta\lambda/\lambda = 10\%$), a source-to-sample distance of 12.8 m, a sample-to-detector distance of 1.5 m for the front detectors and of 13.3 m for the rear detectors, resulting in an available Q-range between $Q_{min} = 0.034$ nm^{-1} and $Q_{max} = 4.98$ nm^{-1} . The micellar samples were prepared either in D_2O (core match) or a D_2O/H_2O 20/80 v/v solution (shell match) and measured in Hellma quartz cuvettes (light path of 1 or 2 mm). The cuvettes were mounted on a thermalised sample changer and measured at three temperatures (T=20°C, 30°C and 40°C). After the first cycle, some of the measurements at T=20°C were repeated to check for reversibility. Samples were measured

in a range of concentrations between 0.1 and 10 polymer wt%. The measuring time was around 15 minutes for the higher concentrations (5-10 wt%) and around 40 minutes for the lower concentrations. The measured intensities were corrected for dark counts, empty cell scattering and put on absolute scale using standard calibration samples after radial averaging. In the fitting routine, the instrument smearing $\Delta Q/Q$ has been taken into account.

Neutron spin echo (NSE)

Neutron spin echo (NSE) experiments were performed at the IN15 beamline at the ILL.[33,34] Four different wavelength have been used (λ = 13.5 Å, 10 Å, 8 Å, and 6 Å) covering a Q range between $Q_{min} = 0.25$ nm^{-1} and $Q_{max} = 2.17$ nm^{-1}, and a Fourier time t range between $t = 50$ ps and $t = 500$ ns. Graphite was used to measure the instrument resolution. Micellar samples were prepared at a polymer concentration of 10 wt% in D_2O in quartz cuvettes with a sample thickness of 2 or 4 mm. The average measuring time was 8 h for each sample. The measurements have been performed at T=20°C, 30°C and 40°C. D_2O measurements with the same cells and instrument configuration as the samples were subtracted as background.

Neutron backscattering (NBS)

Neutron backscattering (NBS) experiments were performed at the Emu beamline at the Australian Nuclear Science and Technology Organization (ANSTO) with a resolution of $\sim$ 1 μeV, equivalent to a time scale of $\sim$ 1 ns (incident wavelength 6.3 Å).[35] The spectra were collected using the full energy transfer range available at the instrument ($\pm$ 30.5 μeV). Samples were loaded in cylindrical aluminium container and measured at two temperatures (20°C and 40°C) for an average measuring time of 8 hours. Data were reduced applying standard corrections, including subtraction of the empty container and vanadium normalization.

Data analysis software

The free software Jscatter[36] was used for data analysis and fitting.

Results and discussion

Rheological properties of block copolymer gels

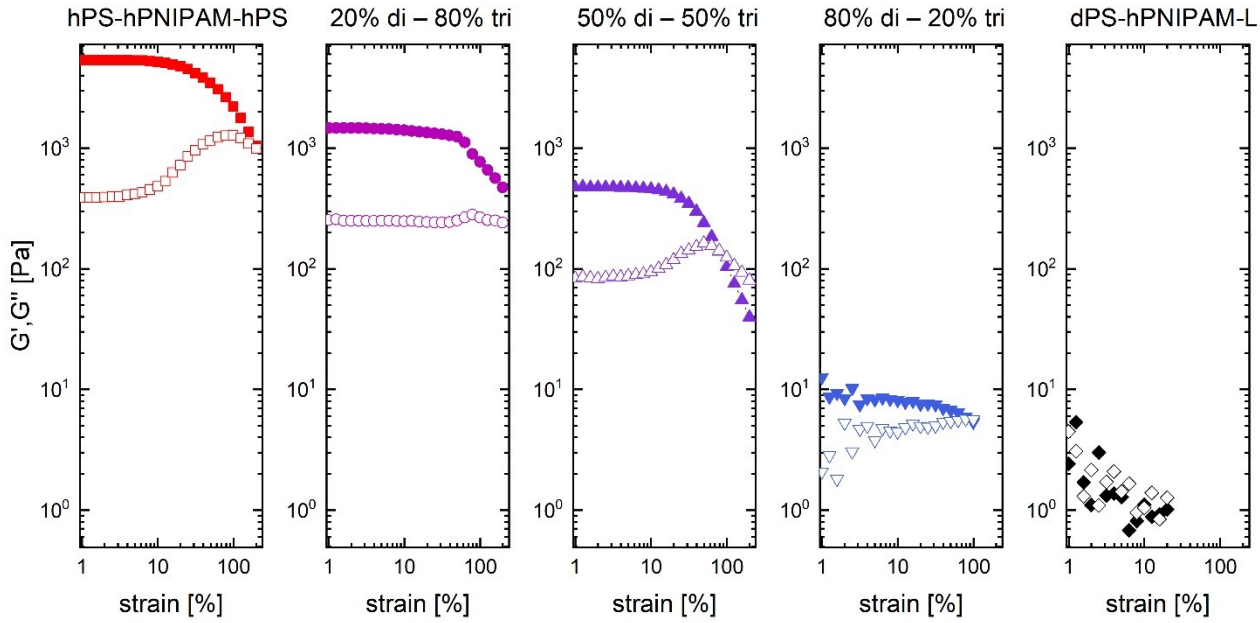

Figure 1: Strain sweep test of micellar samples at 10 wt% of polymer. Full symbols indicate the elastic modulus G' while open symbols represent the loss modulus G''.

The rheological properties of diblock and triblock copolymer micelles have been investigated at a polymer concentration $C_w = 10$ wt% in water. The short and long diblocks (hPS-hPNIPAM-S and hPS-hPNIPAM-L) show respectively a low- and high-viscosity fluid behavior, while the pure triblock (hPS-hPNIPAM-hPS) forms a soft, water-rich gel. Strain sweep tests has been performed on the pure triblock, pure long diblock and diblock/triblock blends (Figure 1). For the pure triblock and the blends, both the elastic modulus G' and the loss modulus G'' show a plateau at low strain, with $G' > G''$, indicating solid-like behaviour. On increasing strain, the elastic modulus starts decaying while the loss modulus exhibits a peak at intermediate strain values followed by a subsequent decrease. The peak value of G'' roughly corresponds to a crossover between storage and loss modulus, above which $G' < G''$. In gel-forming systems, the peak in G'' is associated to a maximum energy dissipation when

the solid starts yielding and cage breaking occurs, with a large number of irreversible particle rearrangements.[37] The relatively high values of yielding point in the triblock sample and in the blends, together with its weak dependence on triblock concentration, suggest that a number of triblocks might bridge different micelles with their outer PS blocks sticking into two different cores, acting as crosslinking points.[38] In this sense we note that even for the sample with the smallest amount of triblocks (80% di - 20% tri) a finite elastic modulus is detected. By contrast, dPS-hPNIPAM-L shows a much poorer mechanical response, even better evidenced by frequency sweep tests (Figure 2) that were performed in the regime where triblock and the blends exhibit a solid-like response (5 % strain). For the 100% triblock sample, the elastic storage modulus G' is almost independent from the frequency ω in the investigated range as expected for solid-like systems. The loss modulus G'' of the 100% triblock and 20% di – 80% tri samples present a shallow minimum in the intermediate frequency range investigated (Figure 2(b)). Such a minimum is often observed in gel-forming systems where it is associated with long-time structural relaxations of particles inside their nearest-neighbour cages.[39]

As the relative content of triblocks decreases, $G'(\omega)$ assumes a stronger dependence on ω that can be described with a power law $G'(\omega) = G'_0\omega^{\Delta}$. The values of the exponent Δ are reported in Figure 2(c) as a function of triblock content $f_{triblock}$. For the reference pure diblock dPS-hPNIPAM-L, the value of Δ is close to the one reported for other polymeric transient networks,[40] whereas the much smaller Δ for the pure triblock system indicates a much stronger network. Furthermore, even for the blend with the smallest amount of triblock (80% di – 20% tri) the storage modulus G' is larger than G'', suggesting high mechanical stability possibly imparted by bringing triblocks acting as crosslinkers.

To quantify the strength of the network formed in triblock-containing samples, we analysed the dependence of $G'_0 \equiv G'(\omega = 0)$ as a function of the relative triblock content $f_{triblock}$. In a purely elastic system, $G'_0(f_{triblock})$ should increase linearly with concentration, whereas in the blends it follows a power law as a function of $f_{triblock}$ (Figure 2(d)). The value of

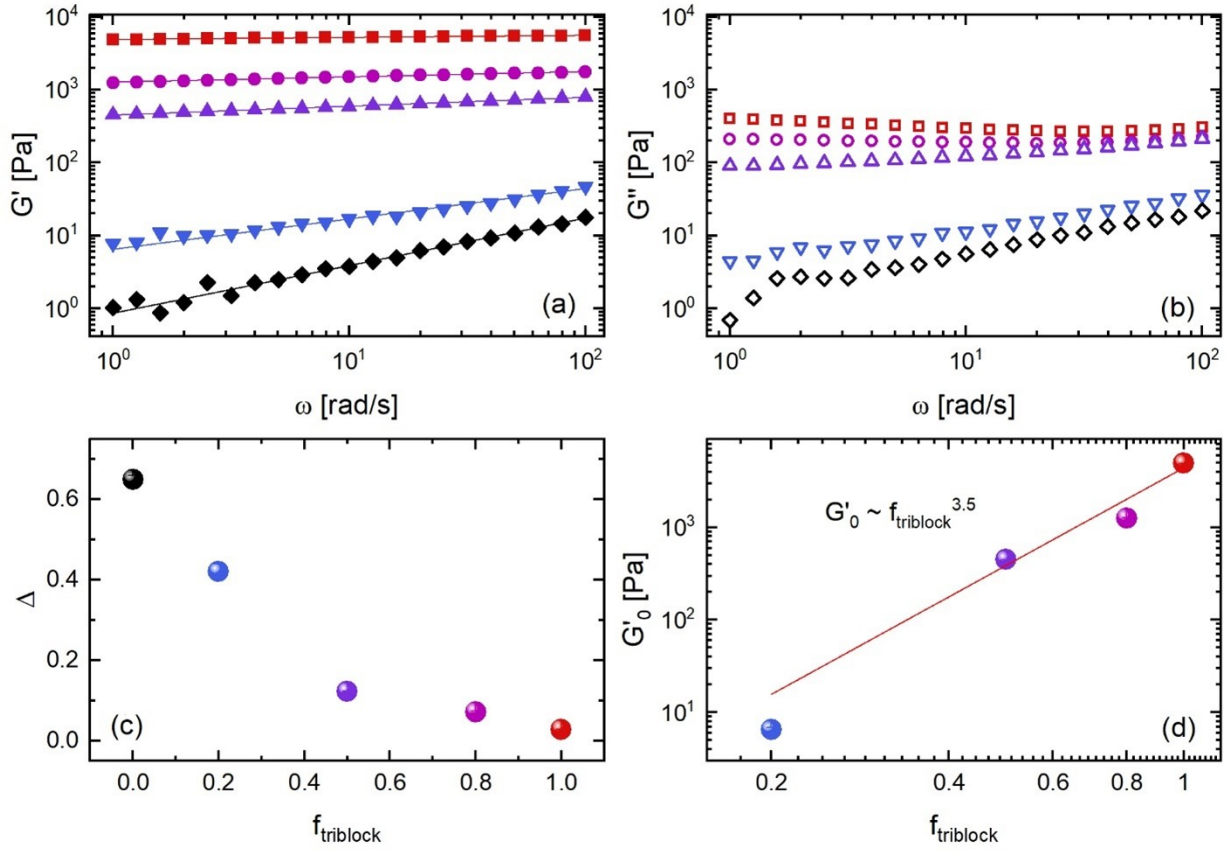

Figure 2: a) Storage modulus G' and b) loss modulus G'' as measured by frequency sweep tests. The symbols and symbol colours have the same meaning as in Figure 1. The solid lines in a) are the fitting curves of the data with the expression $G'(\omega) = G'_0\omega^{\Delta}$. In c) the value of the exponent Δ is reported as a function of the triblock content $f_{triblock}$. The value at $f_{triblock} = 0$ is the one obtained from the fit of dPS-hPNIPAM-L. In d) the dependence of G'_0 as a function of $f_{triblock}$ is fitted with a power law (red line).

the power law exponent ≈ 3.5 is close to that found for other soft gels.[41] In a simple elastic theory, in a system where all the chains are elastically active (i.e., forming bridges) the plateau elastic modulus is given by $G_0 = \rho C_w N_A k_B T/M_w$ with ρ and C_w respectively the polymer density and concentration.[42] This would give a value roughly of $G_0 = 5 \cdot 10^3$ Pa for the triblock system, which is compatible with the value found experimentally. This further suggests that a large number of triblocks are in a bridging configuration.

The weak dependence on frequency of the elastic modulus $G'(\omega)$ seem to indicate that the time scale of bridges formation/rupture is very slow and exceeding the investigated experimental window.[43] It has been estimated[44] that the lifetime of PNIPAM loops formed

by short PS blocks in water is well above 4 ms. This implies that, with respect to the local motions investigated in the subsequent analysis (lying on the nano- and picosecond time scale), the network can be seen as essentially frozen.

Our rheological investigation is consistent with previous studies[7] where PS-PNIPAM-PS triblocks and PS-PNIPAM-PS/PNIPAM blends were found to form stable hydrogels with a relatively high swelling degree. Other authors[22] however found a much poorer mechanical stability in PS-PNIPAM-PS networks. In the latter work the authors directly resuspended the dry materials in water, whereas in our synthesis the samples are gradually passing from an acetone-rich to acetone-poor solution. We assume that the gradual solvent exchange allows a larger number of bridges to be formed, which are kinetically trapped when the polymer is completely dry and subsequently resuspended in pure water. This observation highlights the strong impact of sample preparation protocol for kinetically frozen micelles systems.

To investigate the behaviour above the LCST of PNIPAM, we performed a test frequency sweep measurement for a triblock sample at T=33°C and 39°C (Figure S7). The measurement at higher temperature become critical due to the fast evaporation of water, that cannot be completely prevented due to the small sample interface exposed to air (although the effect has been minimized by covering the exposed interface with a low viscosity oil). On approaching the phase transition (T=33°C), both G' and G'' increase and they show a steeper slope as a function of ω. This means that, on one side, the decreasing solvent quality leads to an enhancement of the number inter- and intra-PNIPAM connections, that strengths the network. On the other side, the PNIPAM shell shrinks and the micelle have thus a larger volume available to execute free motions, leading to a more viscoelastic behaviour.[45] Well above the LCST (T=39°C), the PNIPAM chains shrink until a space-filling network of micelles cannot be maintained anymore.[22] The system thus macroscopically phase separates and the gel breaks down in water-rich and water-poor regions, displaying overall liquid-like behaviour.

Microscopic structure by SANS

PNIPAM homopolymers

We started by investigating the structure of PNIPAM linear chains in solution by SANS, as reference systems. To take into account molecular weight effects, we synthesised chains (PNIPAM10, PNIPAM40 and PNIPAM70) with M_n as close as possible to the equivalent block copolymer (dPS-hPNIPAM-S, dPS-hPNIPAM-L and dPS-hPNIPAM-dPS respectively, see Table 1).

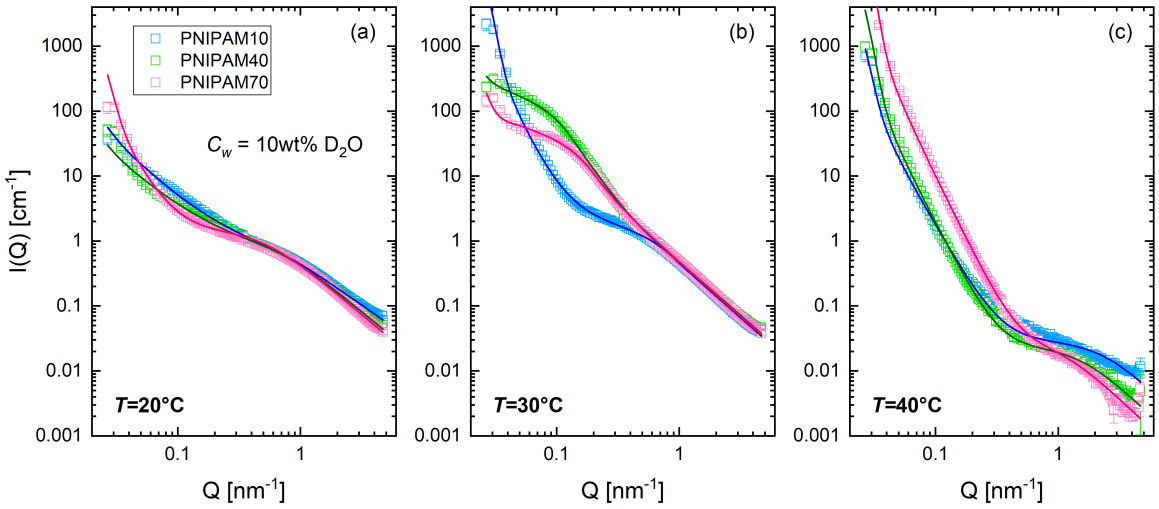

Figure 3: SANS curves for PNIPAM homopolymers at a fixed polymer concentration of C_w=10 wt% in D_2O. Panels a), b), and c) show the data respectively at T=20, 30, and 40°C.

To describe the scattering curves of PNIPAM linear chains we used a generalized Gaussian chain formfactor[46] combined with a power law to describe the observed low Q upturn. Here we recall that the radius of gyration R_g of a polymer chain follows the general scaling law $R_g \sim N^{\nu} l$, with N being the number of segment of length l, and the Flory exponent ν that takes into account for excluded volume effects affecting the chain statistics in solution ($\nu = 1/3$ for collapsed chains, $\nu = 1/2$ for ideal Gaussian chains and $\nu = 3/5$ for swollen chains[46]). The resulting fitting functions are reported in Figure 3 and the corresponding values of R_g in Table S2.

We will now examine the behaviour of the scattering curves at different temperatures. It

is known that the LCST of PNIPAM lies in a temperature interval around 32°C in water, where differences of few degrees are observed depending on parameters as polymer concentration, architecture and solvent composition.[47] Hysteresis curves are also observed during cooling/heating of PNIPAM systems, due to the existence of metastable regions in the phase diagram.[48] To be outside of the hysteresis region it is sufficient to be far enough from the LCST point, i.e. around ± 10°C.

At T=20°C PNIPAM is in the soluble region of its phase diagram, nevertheless the upturn at low Q states the presence of large clusters.[49,50] At T=30°C, the cluster contribution increases. In particular, the formation of mesoscopic structures is observed at intermediate scattering vector Q. We describe the additional contribution through a Guinier-Porod term in the fitting function.[51] The characteristic radius of gyration is on the order of ≈ 8 nm. At T=40°C the power law is dominating, as the inter-chain interactions become more favourable and the system macroscopically phase separate.

Block copolymer micelles

In Figure 4(a), (b), and (c) the SANS curves at T=20°C respectively for dPS-hPNIPAM-S, dPS-hPNIPAM-L and dPS-hPNIPAM-dPS are reported. Samples were measured at three polymer concentrations (1, 5, and 10 wt%) and at two contrasts. Namely, in D_2O/H_2O 20/80 v/v the scattering length density (SLD) of the solvent ($0.83 \cdot 10^{-6}$ Å^{-2}) matches that of the hPNIPAM corona, therefore the scattering from the dPS core is mostly visible, whereas in D_2O (SLD=$6.36 \cdot 10^{-6}$ Å^{-2}) the SLD of the dPS core is matched and the scattering of hPNIPAM corona is highlighted. In shell contrast, at 1 wt% the formfactor $F_{mic}(Q)$ is measured, while at 5 wt% and 10 wt% additionally structure factor contributions in the intermediate Q region are observed. The structure factor peak shifts toward lower Q values as long as the size of the hPNIPAM block increases. At very low Qs a small upturn is observed for all samples, which we ascribe to the formation of aggregates, as in the case of PNIPAM homopolymers.

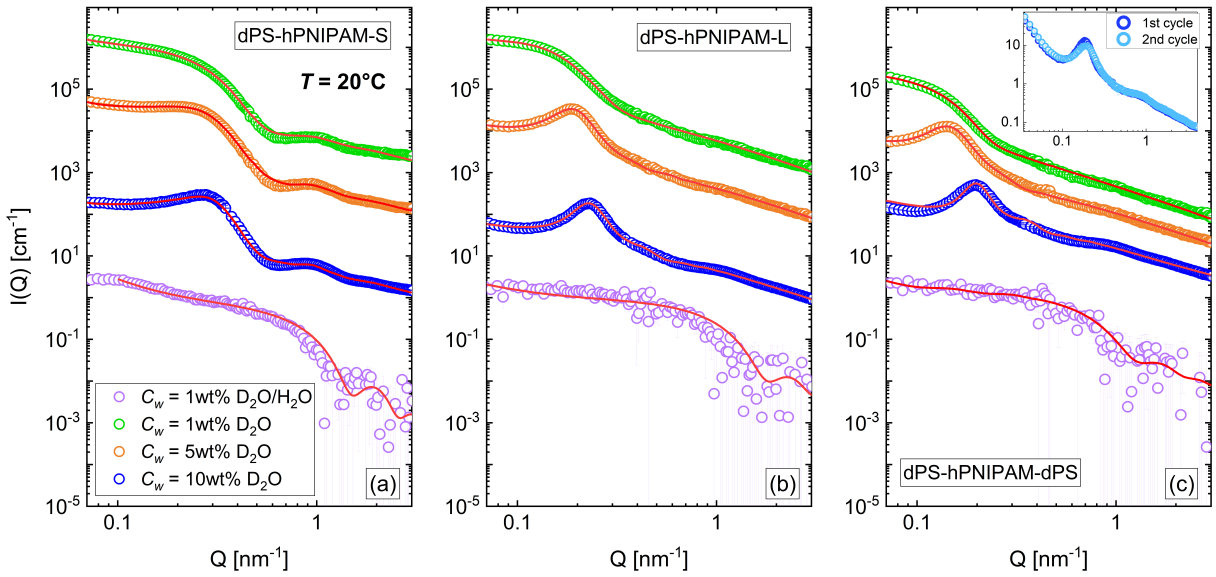

Figure 4: SANS curves for pure block copolymer systems dPS-hPNIPAM-S (a), dPS-hPNIPAM-L (b), and dPS-hPNIPAM-dPS (c) at T=20°C. Data are arbitrarily rescaled for a better comparison. Red lines represent the result of a simultaneous fit using Equation 2 of the Supporting Information. In the inset of (c) the curves for the sample at C_w = 10 wt% are reported before and after heating.

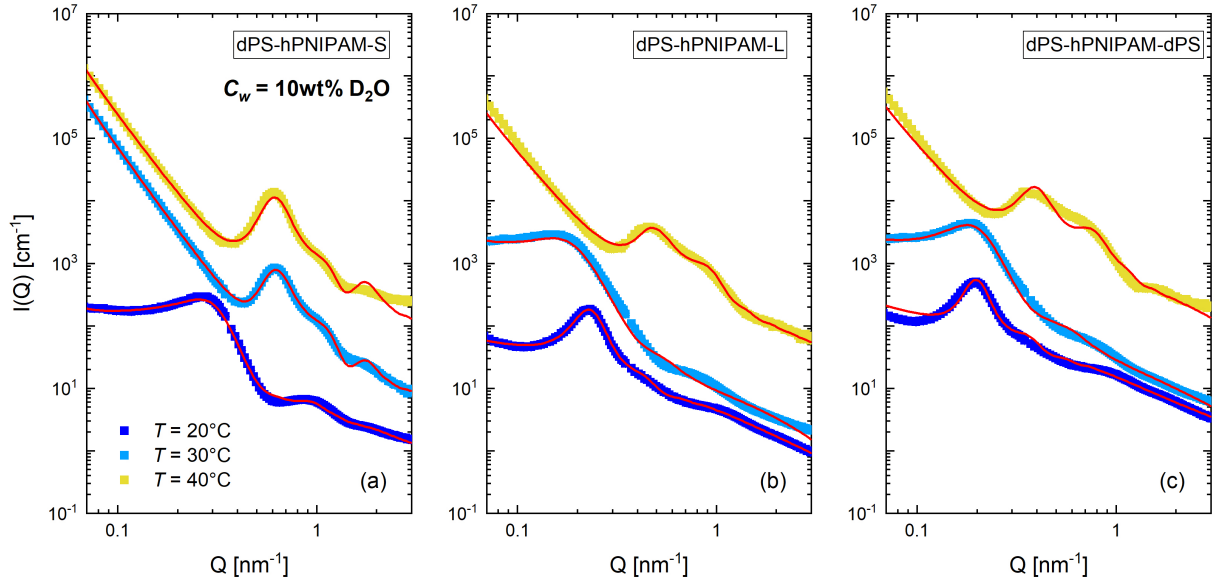

Figure 5: SANS curves for pure block copolymer systems at different temperatures (as indicated in the legend): a) dPS-hPNIPAM-S, b) dPS-hPNIPAM-L, c) dPS-hPNIPAM-dPS. The red curves represent the fitting functions as from Equation 2 of the Supporting Information.

The details of the fitting procedure for the SANS data are reported in the Supporting Information. Here we only recall that the most relevant parameters for the subsequent dynamical analysis are the radius of gyration of PNIPAM $R_g = (l^2 N^{2\nu}/(2\nu+1)(2\nu+2))^{0.5}$, where l and N are respectively the length and number of segments in the PNIPAM block, and ν is the Flory exponent. The resulting fitting functions are reported in Figure 4, and corresponding parameters in Table S3.

We can describe the three block copolymer systems with the same model (chains with one end grafted). This is noteworthy in the triblock case, as we can expect the PNIPAM block either to be in a bridging or loop conformation. The most direct, model-independent approach to visualize the presence of loops is a Kratky plot (see Figure S8). In such a representation, the formfactor of core grafted loops presents a maximum at $QR_{g,loop} \approx 2$ at the same position as isolated loops.[52] For a value of $R_{g,loop} \approx 3$ nm, this would correspond to a maximum around $Q \approx 0.7$ nm^{-1}, however, such maximum does not appear in the measured SANS pattern for the triblock. It could be argued that the characteristic loop maximum is effectively visible only for $\nu \approx 0.5$, and it gets less pronounced for $\nu > 0.5$ as the scattering profile does not get to a plateau but continuously increases on increasing Q. Moreover, in the investigated systems the ring maximum would occur in the Q region where the SANS pattern also shows a typical oscillation due to the spherical arrangement of the grafted chains which is still visible with matched core.

While the oscillation makes it difficult to disentangle the two effects, they give additional information about the distance of the chain from the core: the oscillations shift to smaller Q for the triblocks, indicating that the triblock has a larger distance to the core compared to the linear diblock while the envelope emerging from the PNIPAM chain is maintained. Considering that, for a loop, R_g^2 is half of that of the corresponding linear conformation ($R^2_{g,loop} = R^2_{g,linear}/2$[53]), dominating loop formation should present a peak shift to relatively higher Qs (e.g. taking as reference the linear PNIPAM70 chain, for a $R_{g,linear} = 3.8$ nm we would expect $R_{g,loop} = 2.7$ nm i.e. essentially indistinguishable from the long diblock).

We therefore conclude that SANS confirm what observed by rheology, i.e. that the linear (bridge) configuration is preferred.

Figure 5 compares the scattering pattern in shell contrast at three different temperatures (T=20°C, 30°C, and 40°C). At intermediate temperature (T=30°C), the three polymers show different behaviour: the long diblock and triblock show a similar pattern to that at T=20°C, whereas for the short diblock it is closer to the one at T=40°C. This is probably due to the unfavourable PNIPAM to PS ratio compared to the other two block copolymers, that makes the system overall more hydrophobic and thus shifts the LCST to lower values. At T=40°C, all systems show a strong increase of the forward scattering and a shift of the modulations at high Qs. The first feature is explained by the fact that, above the LCST, the presence of large aggregates is favoured by the increased hydrophobicity of PNIPAM. The latter is due to the shrinking of the corona allowing the micelle cores to come closer to each other.

To fit the data at T=30°C and 40°C, we kept the number of segments N constant for each polymer, as determined from the fit at T=20°C. At T=30°C the number of block copolymer chains per micelle (aggregation number) M increases, as a result of the more hydrophobic character of PNIPAM.[54] This also correlates with the higher connectivity observed by rheology for the triblock network. At T=40°C, the M value remains rather constant and the chain statistics becomes closer to that of a Gaussian chain (ν=0.5), as expected for a system at the LCST.

The micellar structure is preserved at high temperature, as opposed to other reported cases where the micelles dissolve above the LCST.[55] The dissolution is probably hindered in our samples due to the essentially frozen nature of the PS glassy core.[18] The swelling-collapsing process is also fully reversible, as evidenced by the almost perfect superimposition of SANS curves before and after the heating cycle (in the inset of Figure 4(c), the SANS pattern of dPS-hPNIPAM-dPS at 10 wt% is reported as an example).

In Figure 6 the SANS curves of blends of short diblock (dPS-h,dPNIPAM-S) and triblock (dPS-hPNIPAM-dPS) micelles in D_2O (10 wt% of polymer) are reported. In the diblocks

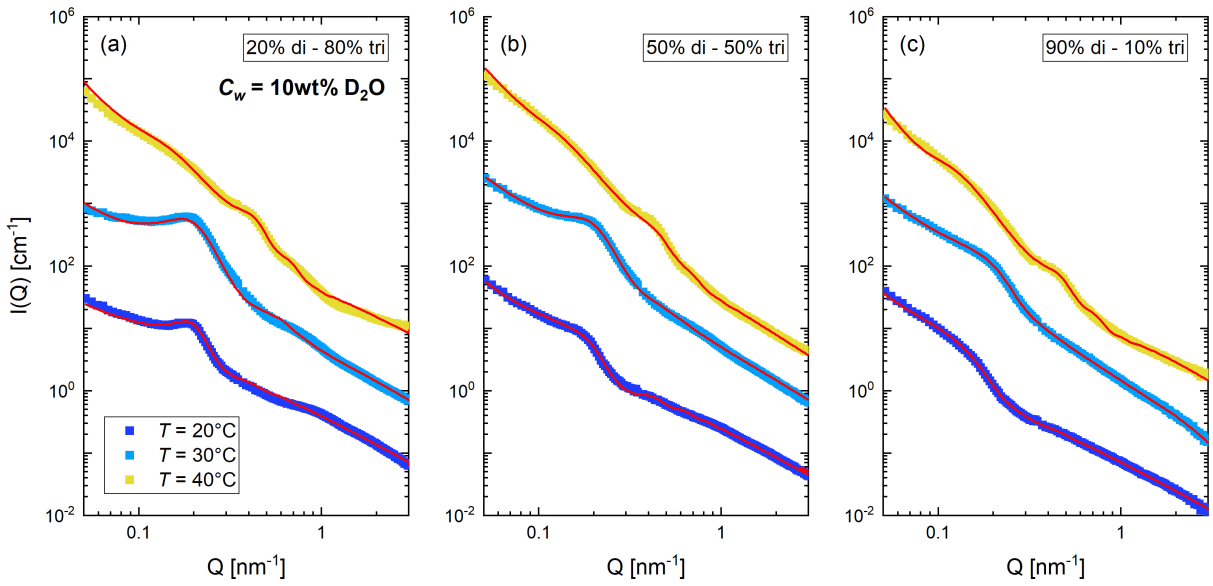

Figure 6: SANS curves for diblock/triblock copolymer blends at different temperatures (as indicated in the legend): a) 20% di - 80% tri, b) 50% di - 50% tri, c) 90% di - 10% tri. The red curves represent the fitting functions as described in the text.

the PNIPAM block is partially deuterated to reach the SLD of D_2O. In this way, we isolate the scattering contribution of the triblocks corona, as we aim to mostly focus on the bridge contribution. The structure factor peak becomes broader as long as we increase the relative amount of matched diblocks, until we see mostly the chain self contribution in the 90% di-10% tri sample. Notably, also in this case there is no signature of a loop formfactor, as mostly visible in a Kratky plot (Figure S8), even at the minimum relative amount of triblocks. This again confirms what is observed by rheology, i.e. that even at low triblock content an elastic response is observed (indicating that the bridge configuration is preferred). To fit the data, we used the same model as for the pure block copolymer systems by fixing the values of l and N to those of the triblock. The resulting values of R_g are reported in Table 3 of the Supporting Information and have been used for the subsequent NSE analysis. Also in this case, the model fits quite well at all temperatures.

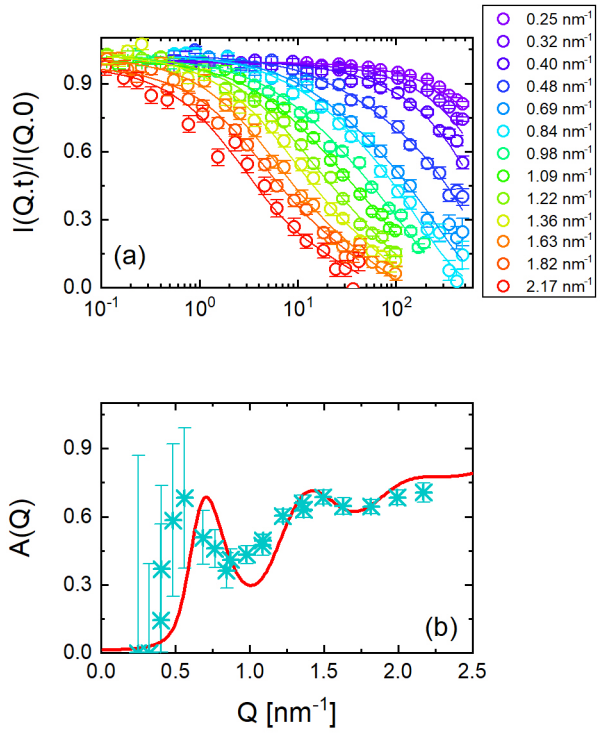

Figure 7: (a) Intermediate scattering functions $I(Q,t)/I(Q,0)$ as measured by NSE at T=20°C for dPS-hPNIPAM-L. Solid lines present the fitting function according to Equation 1. (b) Comparison between $A(Q)$ as obtained from the fit of the NSE data (empty circles) and theoretically calculated according to the mZIF model (red lines).

Micelle diffusion and chain dynamics (NSE)

NSE delivers dynamical information on the length scale covered by the SANS experiment, and on a time scale spanning decades of nanoseconds where both the PNIPAM segmental dynamics and the overall micelle diffusion play a role.[18,23] The observable quantity is the intermediate scattering function (ISF) $I(Q,t)$, normalised to the corresponding value at $t = 0$, $I(Q,t)/I(Q,0)$ (Figure 7(a)). As for the SANS measurements, the SLD of the dPS core mostly matches that of D_2O, thus in the NSE and NBS we mostly focus on the dynamics of hPNIPAM grafted chains. For NSE we report only the analysis at T=20°C and 30°C, since at T=40°C (when dehydration and macroscopic phase separation occur) the dynamic is entirely elastic and the relaxation curves are basically flat (for the short, more hydrophobic block copolymer phase separation occurs already at T=30°C and thus only data at T=20°C

is reported).

The dynamics of a free polymer chain of N segments, with length l, and Flory parameter ν in solution is described by the Zimm model, and can be in principle described by using the structural parameters derived from the SANS analysis. However, the Zimm model often needs to be extended by including internal friction (ZIF model, see Supporting Information).[56–59] Internal friction between neighboring monomers is related to the intrinsic resistance of the polymer to change its conformation, given the existence of energy barriers e.g. for the activation of backbone torsion, methyl rotations, and side-chain movements due to hydrogen bonding, chain collisions, etc.[60] It can be explicitly included in the Zimm model by adding a mode-independent friction time τ_i to each Zimm mode relaxations times $\tau_Z(p) = \tau_Z p^{-3\nu} + \tau_i$.[56] This model well describes the behaviour of linear PNIPAM chains, using the structural parameters from SANS and fitting the parameter τ_i as Q-independent parameter.

For the dynamics of the PNIPAM block in the micelles, we instead use an *ad hoc* model (mZIF) for polymer chains grafted to a micellar core (similarly to the one describing the SANS data) assuming independent dynamics of chains with one fixed end (see the Supporting Information for a detailed discussion). The center-of-mass diffusion is equal to the diffusion of the micelle, while chains present ZIF dynamics. To take into account inter-chain and solvent interactions between micelles, visible in the low-Q region where structure factor effects are relevant, we describe the center-of-mass diffusion coefficient as $D_{cm} = D_0 H(Q)/S(Q)_{exp}$, with $S(Q)_{exp}$ obtained by dividing the SANS intensities of each sample measured at $C_w =$ 10 wt% from the corresponding data at 1 wt%. The diffusion coefficient of the micelle $D_0 = \frac{k_B T}{6\pi\eta R_H}$ has been fixed to that measured by DLS at low concentration. For the hydrodynamic function we used the hard-spheres approximation $H(Q) = 0.75(S(Q)_{exp} - 1) + 1$[61] (the use of such approximations is better justified below). In a first attempt we used the model described so far, by fixing the chain parameters N, l and ν from the SANS analysis (here we recall that $R_g = (l^2 N^{2\nu}/(2\nu+1)(2\nu+2))^{0.5}$). However, to adequately describe the data,

an additional internal elastic term $1 - A(Q)$ had to be considered in the model, i.e.:

$$\frac{I(Q,t)}{I(Q,0)} = e^{-Q^2 D_{cm} t}[(1 - A(Q)) + A(Q)\frac{I_s(Q,t,D_{cm}=0)}{I_s(Q,0,D_{cm}=0)}] \quad (1)$$

with the single chain ISF $I_s(Q,t,D_{cm})$ and micelle center of mass diffusion D_{cm} (see Supporting Information). The resulting fit function together with the experimental data are reported in Figure 7(a). A Q-dependent, long-time plateau $1 - A(Q)$ is observed where the system does not fully relax over the covered time scale, and is sometimes interpreted as the signature of confined motions,[62] as seen for instance in the dynamics of polymer chains grafted on nanoparticles.[63,64] For an ideal micellar structure the internal elastic amplitude $1 - A(Q)$ with chain center of mass at a distance $R + dR_g$ (d is a scaling factor close to unity, that mimic the condition of forbidding core penetration for the chains) is related to the internal dynamic amplitude $A(Q)$ according to our mZIF model (see Supporting Information)

$$A(Q) = \frac{1}{1 + (M-1)sinc^2(Q(R + dR_g))} \quad (2)$$

where M is the number of chains. Figure 7(b) presents the $A(Q)$ from a free fit of the data, in comparison with the theoretical description from Equation 2, including a Gaussian distribution of the parameter $Q(R+R_g)$ to account for polydispersity of R, NSE wavelength distribution, and deviations of the ideal positions of the chains (see Figure S9 for the fit of the three block copolymer systems). Characteristic is the first maximum around $Q(R+R_g) \approx \pi$. At larger Qs, the increasing contribution of chain dynamics is well described from the model. To test the robustness of the fit, we compared the values of $A(Q)$ as obtained by using different approximations: we first tested the differences when fitting $A(Q)$ as free parameter and by fixing the value of $D_{cm}(Q)$ for each Q in terms of $H(Q)$ and $S(Q)$ as described above, by modeling $S(Q)$ either with the experimental value $S(Q)_{exp}$ or the one obtained from the fit of the data with Percus Yervick $S(Q)_{model}$ (as described in the SANS section). We found

that the parameter $A(Q)$ was relatively insensitive to the choice (see Figure S10). We also tried to estimate the goodness of the hard-sphere approximation for $D_{cm}(Q)$, using different assumptions for $S(Q)$ or by fitting $D_{cm}(Q)$ as free parameter (see Figure 10 of Supporting Information). Again, no substantial difference could be found within the error bars. Since the parameters $D_{cm}(Q)$ and $A(Q)$ are correlated, we chose to impose the theoretical model described above for $D_{cm}(Q)$ and fit $A(Q)$ as free parameter. We also checked how the choice affects the other fitting parameters e.g. τ_i and ν, and found them consistent within the error bars. The underestimation of $A(Q)$ at lower Qs might relate to neglecting chain-chain interactions as present in $F'_{eff}(Q)$ in Equation 1 of the Supporting Information.

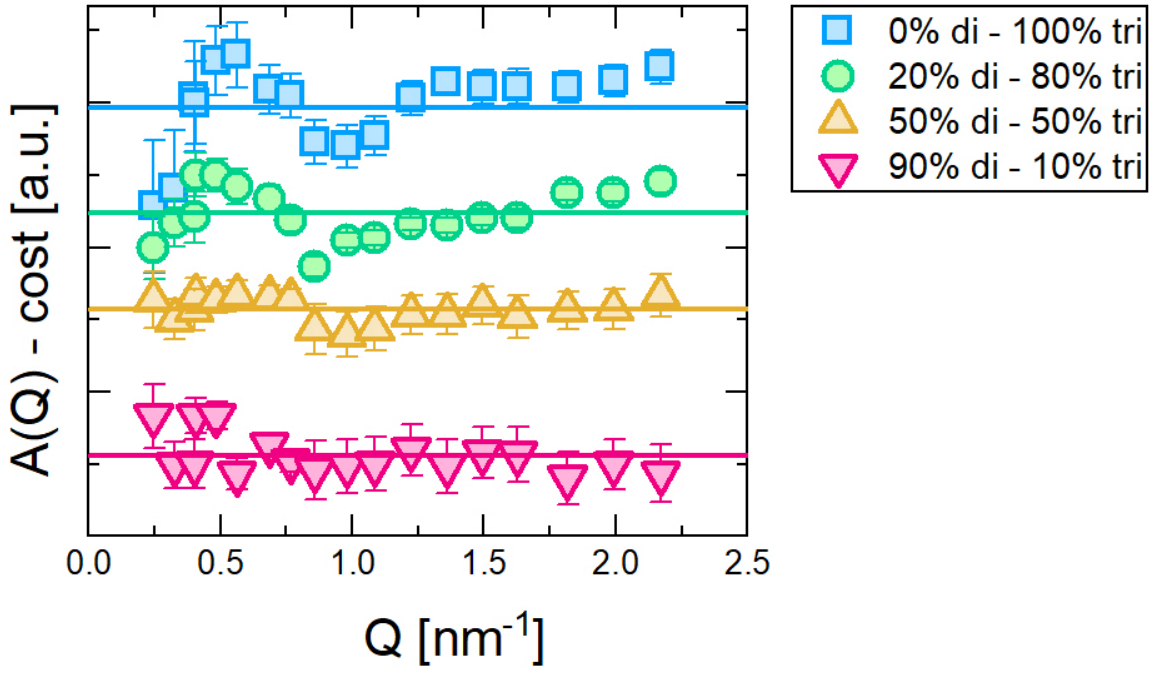

Figure 8: Comparison of $A(Q)$ from different diblock/triblock blends. With decreasing triblock content the visible number of chains M is decreasing reducing the oscillation amplitude. The data have been shifted by a constant term for better clarity.

To further verify the mZIF model we examine the diblock/triblock blends, where the diblock is fully matched to D_2O (as described in the SANS section). The modulation in $A(Q)$ presented in Figure 8 becomes progressively less relevant as the relative amount of

contrast-matched diblocks increases and, correspondingly, the visible number of chains M in Equation 2 decreases. At the lowest triblock concentration we recover a behaviour similar to that of the linear chains in solution.

The mZIF model confirms that the origin of the internal elastic or slow diffusing term in our system is related to static correlations between grafted chains as the average position between grafted chains does not change with time. Despite the uncertainties in the simplified mZIF model, we can conclude that NSE presents internal friction to the tens of nanoseconds for free and grafted chains, as well as for bridging triblocks, and allows to attribute it to backbone torsion. However, the remaining correlations responsible for the modulation in $A(Q)$ are not limited to micelles and should be observed in any configuration where chains are grafted relative to each other, e.g. like on the surface of nanoparticles or polymers in pores.[65] In general, the shape of $A(Q)$ represents the geometry of average positions of grafted chains. In the present case, $A(Q)$ is related to the chain-chain correlation $S_{chain-chain}$ of the micelle formfactor $F_{mic}(Q)$ (Equation 1 of the Supporting Information). Beyond the internal elastic amplitude the observed relaxation corresponds to the single chain relaxations of the grafted ZIF model, as long as the correlations between different chains vanish.

The parameters from the fit of the NSE data of reference PNIPAM chains and block copolymer micelles at T=20°C and T=30°C are reported in Tables S4 and S5. The Zimm time $\tau_Z = \eta R_e^3/(3\pi)^{0.5} k_B T$, where $R_e = lN^\nu$ is the end-to-end distance, is fixed by the SANS analysis, while the internal friction time τ_i is directly obtained from the fit of the NSE data. Due to the large number of parameters in the fit, fixing the structural parameters (and consequently τ_Z) allows in principle to obtain more robust values for other dynamical parameters, in particular τ_i. However, this also introduces an uncertainty on the final value of τ_i which is probably larger than that estimated from the fit, and therefore prevents to realistically discriminate values of τ_i obtained in different samples. With that in mind, we observe that for the linear chains τ_i is on the order of tens of nanoseconds, independently from molecular weight. This is in agreement with simulations[66] that put PNIPAM backbone

torsions on the same time scale. As observed in proteins,[67] an internal friction time $\tau_i \approx \tau_Z$ means that the contribution of internal friction between monomers is orders of magnitude larger than that of solvent friction with a monomer, i.e. dominating (in the case of the short diblock where $\tau_i = \tau_Z$, it would be more than 100 times larger). Similar values of τ_i are found for the block copolymer micelles.

It is worth comparing our analysis with that of Adelbserger *et al.*[18,23] that investigated similar PS-PNIPAM micellar systems with NSE. The authors described the scattering functions using an empirical model of two additive contributions, with a faster one related to the chain dynamics and a slower one to the overall micelle diffusion (neglecting the coupling between chain dynamics and the micellar core). They observed a decreasing rate for $\tau_{eff} \sim Q^{-2}$ slower than Q^{-3} predicted by the Zimm model, that they associated with the onset of a collective breathing mode of the PNIPAM corona. In our case we would not expect such a strong coupling that is generally observed only at very high grafting density[68] $g = M/4\pi R^2$, while in our micelles g is relatively small ($g \approx 0.5$ nm^{-2}). The analysis from Adelbserger *et al.* is focused in the Q region between 0.8 nm^{-1} and 1.8 nm^{-1}. In such a high Q region, we anyhow expect a slower rate than that predicted from Zimm, due to internal friction ($\tau_{eff} \sim Q^{-2}$). This can be more easily observed by looking at the effective diffusion coefficient D_{eff}, as obtained by fitting the scattering functions with $\frac{I(Q,t)}{I(Q,0)} \sim e^{-Q^2 D_{cm} t}[(1-A(Q))+A(Q)e^{-Q^2 D(Q) t}]$, $D_{eff} = D_{cm} + D(Q)$ (Figure 9). While Zimm predicts $D_{eff} \sim Q$, internal friction leads to a reduced slope and to a plateau at high Qs (as especially evident for the triblock case). We therefore conclude that, in the investigated system, the slowing down at high Q does not evidence an additional breathing mode but it can be well explained by internal friction.

A final consideration can be made on how the presence of loops would influence the analysis of the NSE data. In this case, to discriminate between loops or bridges would require the possibility to discriminate between a mZIF model with one or two fixed ends respectively. However, the current model cannot discriminate between one or two fixed ends as already the single chain contributions are almost equal. We thus conclude that the

NSE analysis alone cannot exclude the presence of loops (but their absence is supported by rheology and SANS, as discussed above).

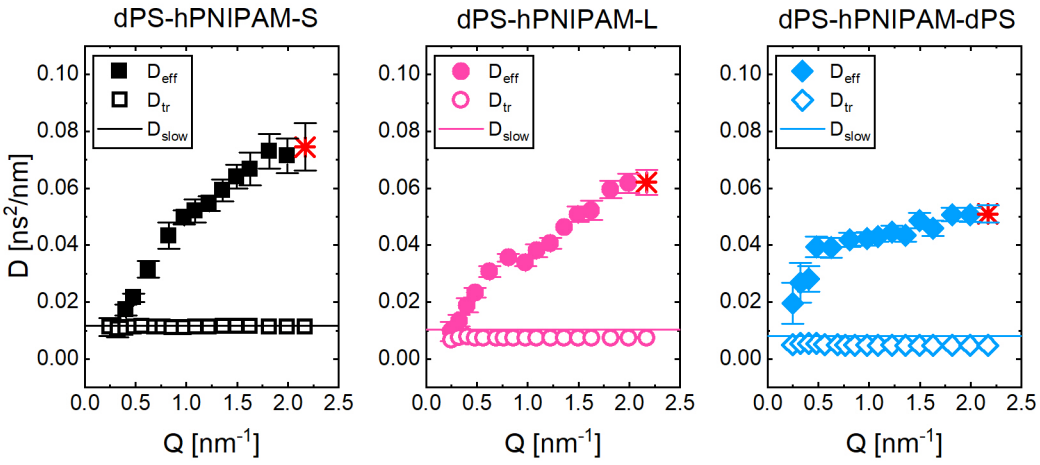

Figure 9: Full symbols: effective diffusion coefficient D_{eff}. The red star marks the value that has been used for the analysis of the NBS data. Open symbols: translational diffusion coefficient, corrected of structure factor effects. Solid line: diffusion coefficient of the core as observed on NBS.

Local chain dynamics (NBS)

Compared to NSE, with NBS we probe the dynamics of PNIPAM protons at higher Qs and shorter time scales. Here the Zimm description, which is essentially a coarse-grained model, is less adequate as we start to see the details of the chain segments. In a NBS experiment, the incoherent (self) dynamics of protons is usually assumed to be the most relevant contribution, as the incoherent scattering cross section of hydrogen is much larger that the other atoms in the system.

In Figure 10 we report the dynamic structure factor $S(Q, \hbar\omega)$ of one sample (dPS-hPNIPAM-S), at two different temperatures and two different Qs as exemplary case. Below the LCST (T=20°C), a quasielastic signal is observed, whereas at T=40°C the signal is mostly elastic. This is in line with what we observed on the NSE window, and has been detected by experimental[69] and computational[66] methods for other PNIPAM systems on the backscattering time and length scales. Namely, a strongly reduced mobility above the LCST

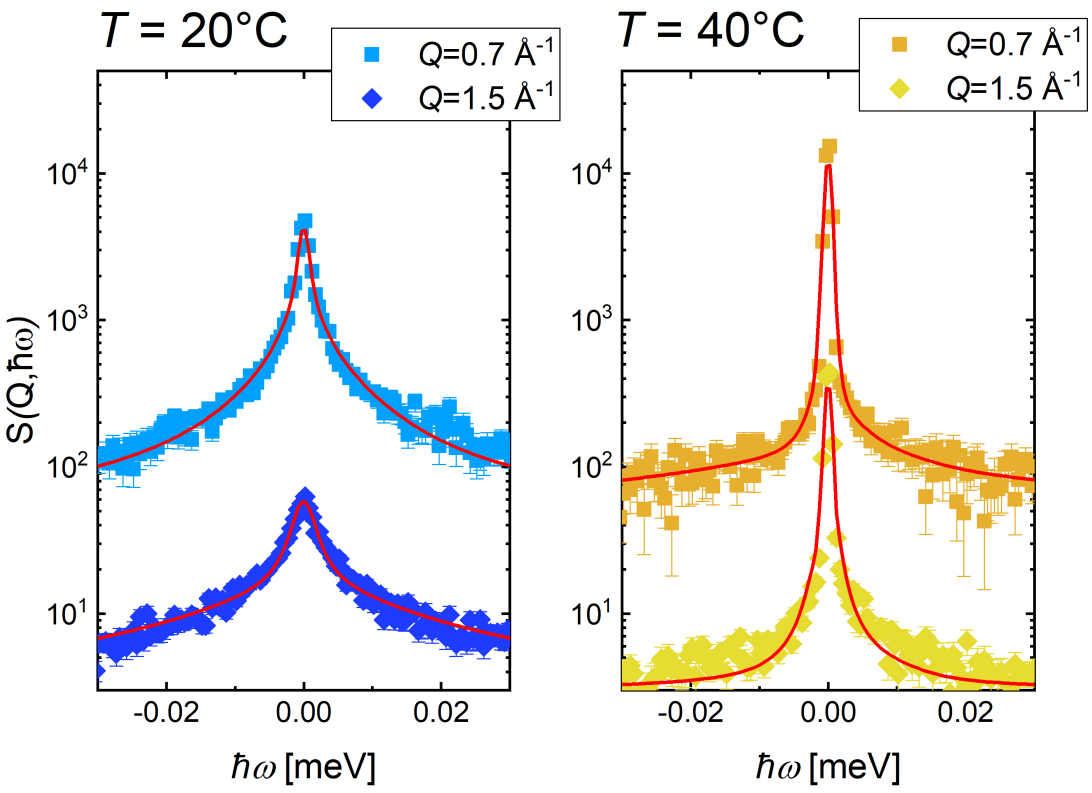

Figure 10: NBS spectra (symbols) and fit (solid lines) for dPS-hPNIPAM-S at two temperatures and two different Qs.

is observed due to partial dehydration of the chain and aggregation.

We first focus on low temperature (T=20°C). To describe the dynamics of PNIPAM side chain protons, we use the approach first developed by Volino[70] that models soft confinement as diffusion in a harmonic potential:

$$
\begin{aligned}
S_{harm}(Q,\hbar\omega,\langle u_x^2\rangle,\tau_h) &= A_0(Q) + \sum_n A_n(Q) L(\hbar\omega, n/\tau_h) \\
A_0(Q) &= e^{-Q^2\langle u_x^2\rangle} \\
A_n(Q) &= e^{-Q^2\langle u_x^2\rangle}\frac{(Q^2\langle u_x^2\rangle)^n}{n!}
\end{aligned}
\tag{3}
$$

i.e. as a sum of an elastic term $A_0(Q)$ and an inelastic term dependent on the correlation time τ_h and mean square displacements $\langle u_x^2\rangle$ in the harmonic potential assuming $\langle u_x^2\rangle$ =

$\langle u_y^2 \rangle = \langle u_z^2 \rangle = \langle u^2 \rangle / 3$. $L(\hbar\omega, \gamma)$ is the Lorentzian function $L(\hbar\omega, \gamma) = \frac{\gamma}{\pi(\hbar^2\omega^2 + \gamma^2)}$. We also take into account the fast contribution of methyl rotations, that in the time domain has the form:

$$I_{meth}(Q,t) = (EISF + (1 - EISF)e^{-(t/t_0)^\beta}) \tag{4}$$

with $EISF = \frac{1}{3} + \frac{2}{3} sin(QR_{HH})/(QR_{HH})$, where R_{HH} is the proton-proton jump distance and t_0 the residence time. In the analysis we fixed R_{HH}=1.2 Å, t_0 = 1 ps and $\beta = 0.8$.[71] To describe the dynamics of PNIPAM side chains we use:

$$S_{SC}(Q,\hbar\omega) = S_{harm}(Q,\hbar\omega) \otimes (f_{meth} \cdot FT[I_{meth}(Q,t)] + (1 - f_{meth}) \cdot \delta(\hbar\omega)) \tag{5}$$

where FT indicates the Fourier transform in time domain, and with the fraction of methyl protons in the side chain $f_{meth} \equiv 6/7$.

The NSE analysis showed that backbone segment dynamics is slowed down to the scale of tens of nanoseconds by internal friction and an additional center of mass diffusion. We therefore assume that a fraction of slow diffusing protons contribute to the overall NBS signal, i.e. we assume the following form for the scattering function for PNIPAM segments:

$$S_{PNIPAM}(Q,\hbar\omega) = [(1 - f) \cdot \delta(\hbar\omega) + f \cdot S_{SC}(Q,\hbar\omega)] \otimes L(\hbar\omega, D_\infty Q^2) \tag{6}$$

with $f \equiv 7/10$ the fraction of protons in the side chain. The overall diffusion of the PNIPAM chain[72] was included with $D_\infty Q^2$, where D_∞ is the effective diffusion observed at the highest Q on NSE (the corresponding value is marked in Figure 9). To better reproduce the data, an additional term describing the contribution from the glassy PS in the core was needed.[18] Such a contribution is expected to be small due to the small incoherent contribution of the dPS block. Indeed, in the final fit such contribution turned out to be a relatively small fraction of the overall intensity (fraction of slow component $f_s \lessapprox 20\%$) and it decreases as long as the ratio between the size of PNIPAM and PS blocks increases. The associated

diffusion coefficient is approximately $\approx D_0$ (the actual values are reported in Figure 9). The overall fitting function has been described as:

$$S(Q,\hbar\omega) = \alpha(Q)[f_s \cdot S_{PNIPAM}(Q,\hbar\omega) + (1-f_s)L(Q,\hbar\omega,D_0Q^2) + bgk] \otimes R(Q,\hbar\omega) \quad (7)$$

where $\alpha(Q)$ contains vibrational contributions (Debye-Waller) and the background has been modeled as a very broad Lorentzian (taking into account that the D_2O signal on Emu appears as a very broad Lorentzian at the lowest Qs, or essentially flat in the rest of the Q range). The resolution function $R(Q,\hbar\omega)$ was modeled as a sum of Gaussian functions determined from a vanadium measurement.

The parameters obtained from the fit of the NBS data at T=20°C and 30°C with the model described in Equation 7 are reported respectively in Tables S6 and S7. The analysis shows that the side chain protons move with root mean square displacements (RMSD) $\langle u_x^2 \rangle^{0.5} \equiv u_0 \approx 2$ Å and a relaxation time τ_h around 100 ps. The RMSD are smaller than the sidechain extension from C_α carbon to the methyl groups of 4.3-5 Å, and the timescale is in agreement to what found by simulations for sidechain oscillations.[66] We thus observe localised motions where the side chains stay in same orientation to the backbone that do not include backbone rotations, as these would require RMSD larger than the sidechain extension. In the blends, the correlation time decreases with decreasing triblock content. This might indicate that at high triblock content (gel state) the mobility of PNIPAM side chains is slowed down, for example, by the formation of a larger number of PNIPAM-PNIPAM hydrogen bonds.

Above the LCST (T=40°C) the spectra drastically change as the signal becomes mostly elastic. We thus fit the data with the convolution of an harmonic term and a methyl group contribution (the translational component gets too slow and small to contribute), plus background. In this case the data are well described assuming a small fraction of mobile protons

(around 20% from the fit). The fast dynamics on the order of tens of ps is localised on a scale of ≈ 2 Å. Namely, above the transition only fast side chain motions are active, whereas the overall mobility is drastically reduced by chain collapse and generation of a melt of bare polymer chains at the LCST.[73]

Conclusions

In this work we investigated PS-PNIPAM diblock- and PS-PNIPAM-PS triblock copolymer micelles at high concentration in water, as model thermoresponsive hydrogels. Below the LCST, at the same polymer concentration, a higher viscous liquid is formed for PS-PNIPAM diblocks as long as the size of the PNIPAM block increases, however, a proper gel state is formed when even a small amount of triblocks is added to the system. This is likely due to the possibility of triblocks to form junctions bridging different micellar cores. On a microscopic scale, the structural features are well described by a non-centrosymmetric model of chains with one end grafted on a spherical core, independently of PNIPAM block size and architecture (diblock, triblock). This confirms that the majority of triblocks are engaged in bridge formation (low amount of loops).

The intermediate-scale chain dynamics (as seen by NSE) is well described by a new approach, combining the Zimm model with internal friction (ZIF) with the topological constrains induced by fixing the chains to the micellar core and an additional elastic contribution that results from static correlation between grafted chains (mZIF). This shows that the "soft" confinement provided by the low grafting density and crosslinking can be treated as a relatively simple correction to the model of a free chain in solution. The internal friction on the order of tens of nanoseconds is in agreement with previous simulations that put backbone torsion on the same scale.

Additional information is provided by the analysis of PNIPAM dynamics on shorter time and length scales by NBS. The evaluation confirms that backbone dynamics is mostly frozen

on the nanosecond time scale due to internal friction, whereas side chains are mobile on the times scale of hundreds of picoseconds and length scale of few angstrom.

On approaching the LCST, the elastic response initially increases indicating that a larger number of micelles are connected. The LCST is slightly decreased in short diblocks compared to pure PNIPAM, due to the overall more hydrophobic character. Well above the LCST, the systems macroscopically phase separate in highly cross-linked, polymer-rich regions and water-rich regions, although the local micellar structure is preserved. The mobility of PNIPAM is strongly reduced even at the chain level, as the side chains get mostly dehydrated and only very fast motions (as methyl rotations) remain active.

The process is largely reversible and the micellar structure is preserved as the system is cooled down below the LCST. This is probably related to the glassy nature of the PS core, making the system more similar to frozen nanoparticles than dynamic micelles. In particular, the lifetime of the triblock junctions is orders of magnitude slower than the characteristic times of the underlying chain dynamics, i.e. the two processes (bridge formations and chain motions) are completely decoupled, resembling more a chemical rather than physical cross-linked hydrogel.

Overall, analyzing macroscopic rheology and microscopic structure (SANS) and dynamics (NSE,NBS) data we find evidence that the majority of triblocks engage in intermicellar junctions, but their structure and dynamics are quite similar to those of a PNIPAM hydrated chain. The theoretical framework developed to describe the local mobility, from micelle diffusion down to segmental and side chain dynamics, can find future application in the microscopic description of other nanoscale-structured systems and "permanent" networks, especially when details on the connection between local architecture and dynamics are lacking.

Supporting Information

The following Supporting Information is available: Supplementary synthesis materials and methods; Supplementary rheological data; Supplementary SANS analysis; Supplementary theoretical section; Supplementary NSE analysis; Supplementary NBS analysis

Acknowledgement

The authors acknowledge the Australian Centre for Neutron Scattering and ANSTO for supporting the neutron research infrastructure used in this work via ACNS Proposal No. 16648, and the Institut Laue-Langevin for beamtime allocation. B. R. and S. F. acknowledge financial support from the German Science Foundation (DFG) via SFB 985.

References

(1) Khan, M. U. A.; Stojanović, G. M.; Abdullah, M. F. B.; Dolatshahi-Pirouz, A.; Marei, H. E.; Ashammakhi, N.; Hasan, A. Fundamental properties of smart hydrogels for tissue engineering applications: A review. *International Journal of Biological Macromolecules* **2024**, *254*, 127882.

(2) Bordbar-Khiabani, A.; Gasik, M. Smart Hydrogels for Advanced Drug Delivery Systems. *International Journal of Molecular Sciences* **2022**, *23*, 3665.

(3) Sikdar, P.; Uddin, M. M.; Dip, T. M.; Islam, S.; Hoque, M. S.; Dhar, A. K.; Wu, S. Recent advances in the synthesis of smart hydrogels. *Mater. Adv.* **2021**, *2*, 4532–4573.

(4) Wei, M.; Gao, Y.; Li, X.; Serpe, M. J. Stimuli-responsive polymers and their applications. *Polym. Chem.* **2017**, *8*, 127–143.

(5) Zhang, K.; Xue, K.; Loh, X. J. Thermo-responsive hydrogels: from recent progress to biomedical applications. *Gels* **2021**, *7(3)*, 77.

(6) Gou, S.; Porcello, A.; Allémann, E.; Salomon, D.; Micheels, P.; 3, O. J.; Kalia, Y. N. Injectable hyaluronan-based thermoresponsive hydrogels for dermatological applications. *Pharmaceutics* **2023**, *15(6)*, 1708.

(7) Nykänen, A.; Nuopponen, M.; Laukkanen, A.; Hirvonen, S.-P.; Rytelä, M.; Turunen, O.; Tenhu, H.; Mezzenga, R.; Ikkala, O.; ; Ruokolainen, J. Phase Behavior and Temperature-Responsive Molecular Filters Based on Self-Assembly of Polystyrene-block-poly(N-isopropylacrylamide)-block-polystyrene. *Macromolecules* **2007**, *40(16)*, 5827–5834.

(8) Sridhar, S. P.; Soman, A. K.; Sankaran, T. S.; Chandran, S.; Joseph, B. Temperature responsive poly (N-isopropylacrylamide-block-styrene) block copolymer coatings with tunable hydrophilicity. *Surfaces and Interfaces* **2020**, *21*, 100800.

(9) Kirkland, S. E.; Hensarling, R. M.; McConaughy, S. D.; Guo, Y.; Jarrett, W. L.; McCormick, C. L. Thermoreversible hydrogels from RAFT-synthesized BAB triblock copolymers: steps toward biomimetic matrices for tissue regeneration. *Biomacromolecules* **2008**, *9*, 481–486.

(10) Mocan, M.; de Grooth, J.; Hofman, A. H.; van der Kooij, H. M.; Loos, K.; de Vos, W. M.; ; Kamperman, M. Free-standing thermo-responsive nanoporous membranes from high molecular weight PS-PNIPAM block copolymers synthesized via RAFT polymerization. *Polym. Chem.* **2017**, *8*, 2235–2243.

(11) Xu, F.; Xu, J.-W.; Zhang, B.-X.; Yan-Ling, L. Self-assembly micelles from novel triarmed star C3-(PS-b-PNIPAM) block copolymers for anticancer drug release. *AIChE Journal* **2015**, *61*, 35–45.

(12) Wu, J.; Li, H.; Zhang, N.; Zheng, Q. Micelle-Containing Hydrogels and Their Applications in Biomedical Research. *Gels* **2024**, *10*, 471.

(13) Ganguly, R.; Kumar, S.; Kunwar, A.; Nath, S.; Sarma, H.; Tripathi, A.; Verma, G.; Chaudhari, D.; Aswal, V.; Melo, J. Structural and therapeutic properties of curcumin solubilized pluronic F127 micellar solutions and hydrogels. *J. Mol. Liq.* **2020**, *314*, 113591.

(14) Tamate, R.; Hashimoto, K.; Horii, T.; Hirasawa, M.; Li, X.; Shibayama, M.; Watanabe, M. Self-healing micellar ion gels based on multiple hydrogen bonding. *Adv. Mat.* **2018**, *30*, 1802792.

(15) Jiang, J.; Li, C.; Lombardi, J.; Colby, R. H.; Rigas, B.; Rafailovich, M. H.; Sokolov, J. C. The effect of physiologically relevant additives on the rheological properties of concentrated Pluronic copolymer gels. *Polymer* **2008**, *49*, 3561–3567.

(16) Nicolai, T.; Colombani, O.; Chassenieux, C. Dynamic polymeric micelles versus frozen nanoparticles formed by block copolymers. *Soft Matter* **2010**, *6*, 3111–3118.

(17) Nuopponen, M.; Ojala, J.; Tenhu, H. Aggregation behaviour of well defined amphiphilic diblock copolymers with poly (N-isopropylacrylamide) and hydrophobic blocks. *Polymer* **2004**, *45*, 3643.

(18) Adelsberger, J.; Meier-Koll, A.; Bivigou-Koumba, A. M.; Busch, P.; Holderer, O.; Hellweg, T.; Laschewsky, A.; Müller-Buschbaum, P.; Papadakis, C. M. The collapse transition and the segmental dynamics in concentrated micellar solutions of P(S-b-NIPAM) diblock copolymers. *Colloid Polym Sci* **2011**, *289*, 711–720.

(19) Zhang, W.; Zhou, X.; Li, H.; Fang, Y.; Zhang, G. Conformational Transition of Tethered Poly(N-isopropylacrylamide) Chains in Coronas of Micelles and Vesicles. *Macromolecules* **2005**, *38(3)*, 909–914.

(20) Zhou, X.; Ye, X.; Zhang, G. Thermoresponsive triblock copolymer aggregates investigated by laser light scattering. *J. Phys. Chem. B* **2007**, *111*, 5111–5115.

(21) Jain, A.; Kulkarni, A.; Koumba, A. M. B.; Wang, W.; Busch, P.; Laschewsky, A.; Müller-Buschbaum, P.; Papadakis, C. M. Micellar Solutions of a Symmetrical Amphiphilic ABA Triblock Copolymer with a Temperature-Responsive Shell. *Macromolecular Symposia* **2010**, *291-292*, 221–229.

(22) Bivigou-Koumba, A. M.; Görnitz, E.; Laschewsky, A.; Müller-Buschbaum, P.; Papadakis, C. M. Thermoresponsive amphiphilic symmetrical triblock copolymers with a hydrophilic middle block made of poly(N-isopropylacrylamide): synthesis, self-organization, and hydrogel formation. *Colloid Polym. Sci.* **2010**, *288*, 499–517.

(23) Adelsberger, J.; Kulkarni, A.; Jain, A.; Wang, W.; Bivigou-Koumba, A. M.; Busch, P.; Pipich, V.; Holderer, O.; Hellweg, T.; Laschewsky, A.; Müller-Buschbaum, P.; Papadakis, C. M. Thermoresponsive PS-b-PNIPAM-b-PS Micelles: Aggregation Behavior, Segmental Dynamics, and Thermal Response. *Macromolecules* **2010**, *43*, 2490–2501.

(24) Adelsberger, J.; Metwalli, E.; Diethert, A.; Grillo, I.; Bivigou-Koumba, A. M.; Laschewsky, A.; Müller-Buschbaum, P.; Papadakis, C. M. Kinetics of Collapse Transition and Cluster Formation in a Thermoresponsive Micellar Solution of P(S-b-NIPAM-b-S) Induced by a Temperature Jump. *Macromol. Rapid Commun.* **2012**, *33*, 254–259.

(25) Papagiannopoulos, A.; Zhao, J.; Zhang, G.; Pispas, S.; Radulescu, A. Thermoresponsive aggregation of PS–PNIPAM–PS triblock copolymer: a combined study of light scattering and small angle neutron scattering. *Eur. Polym. J.* **2014**, *56*, 59–68.

(26) Liu, J.; Xu, W.; Kuang, Z.; Dong, P.; Yao, Y.; Wu, H.; Liu, A.; Ye, F. Gradient porous PNIPAM-based hydrogel actuators with rapid response and flexibly controllable deformation. *J. Mater. Chem. C* **2020**, *8*, 12092–12099.

(27) Ohya, S.; Kidoaki, S.; Matsuda, T. Poly(N-isopropylacrylamide) (PNIPAM)-grafted gelatin hydrogel surfaces: interrelationship between microscopic structure and mechan-

ical property of surface regions and cell adhesiveness. *Biomaterials* **2005**, *26*, 3105–3111.

(28) Grimm, A.; Nowak, C.; Hoffmann, J.; Schärtl, W. Electrophoretic Mobility of Gold Nanoparticles in Thermoresponsive Hydrogels. *Macromolecules* **2009**, *42*, 6231–6238.

(29) Caccavo, D.; Cascone, S.; Lamberti, G.; Barba, A. A. Hydrogels: experimental characterization and mathematical modelling of their mechanical and diffusive behaviour. *Chem. Soc. Rev.* **2018**, *47*, 2357–2373.

(30) Huang, Y.; Morozova, S. M.; Li, T.; Li, S.; Naguib, H. E.; Kumacheva, E. Stimulus-responsive transport properties of nanocolloidal hydrogels. *Biomacromolecules* **2023**, *24(3)*, 1173–1183.

(31) Yavitt, B. M.; Salatto, D.; Zhou, Y.; Huang, Z.; Endoh, M.; Wiegart, L.; Bocharova, V.; Ribbe, A. E.; Sokolov, A. P.; Schweizer, K. S.; Koga, T. Collective Nanoparticle Dynamics Associated with Bridging Network Formation in Model Polymer Nanocomposites. *ACS Nano* **2021**, *15*, 11501–11513.

(32) Costa, R. O. R.; Freitas, R. F. S. Phase behavior of poly(N-isopropylacrylamide) in binary aqueous solutions. *Polymer* **2002**, *43*, 5879–5855.

(33) Rosi, B. P.; Allgaier, J.; Czakkel, O.; Förster, S.; Holderer, O.; Kruteva, M.; Prevost, S.; Schwärzer, K. **2023**, doi:10.5291/ILL–DATA.9–10–1735.

(34) Rosi, B. P.; Allgaier, J.; Biehl, R.; Czakkel, O.; Holderer, O.; Kruteva, M.; Prevost, S.; Robledo, J. **2024**, doi:10.5291/ILL–DATA.9–10–1830.

(35) de Souza, N. R.; Klapproth, A.; and, G. N. I. EMU: High-Resolution Backscattering Spectrometer at ANSTO. *Neutron News* **2016**, *27*, 20–21.

(36) Biehl, R. Jscatter, a program for evaluation and analysis of experimental data. *PLoS One* **2019**, *14(6)*, e0218789.

(37) N. Koumakis, A. S. P., A. Pamvouxoglou; Petekidis, G. Direct comparison of the rheology of model hard and soft particle glasses. *Soft Matter* **2012**, *8*, 4271–4284.

(38) Thuresson, K.; Nilsson, S.; Kjøniksen, A.-L.; Walderhaug, H.; Lindman, B.; Nyström, B. Dynamics and rheology in aqueous solutions of associating diblock and triblock copolymers of the same type. *J. Phys. Chem. B* **1999**, *103(9)*, 1425–1436.

(39) Laurati, M.; Petekidis, G.; Koumakis, N.; Cardinaux, F.; Schofield, A. B.; Brader, J. M.; Fuchs, M.; Egelhaaf, S. U. Structure, dynamics, and rheology of colloid-polymer mixtures: From liquids to gels. *J. Chem. Phys.* **2009**, *130*, 134907.

(40) Aamer, K. A.; Sardinha, H.; Bhatia, S. R.; Tew, G. N. Rheological studies of PLLA–PEO–PLLA triblock copolymer hydrogels. *Biomaterials* **2004**, *25(6)*, 1087–1093.

(41) Stavrouli, N.; Aubry, T.; Tsitsilianis, C. Rheological properties of ABA telechelic polyelectrolyte and ABA polyampholyte reversible hydrogels: A comparative study. *Polymer* **2008**, *49*, 1249–1256.

(42) Lei, Y.; Lodge, T. P. Effects of component molecular weight on the viscoelastic properties of thermoreversible supramolecular ion gels via hydrogen bonding. *Soft Matter* **2012**, *8*, 2110–2120.

(43) Berret, J.-F.; Calvet, D.; Collet, A.; Viguier, M. Fluorocarbon associative polymers. *Current Opinion in Colloid and Interface Science* **2003**, *8*, 296–306.

(44) Cui, S.; Liu, C.; Zhang, W.; Zhang, X.; Wu, C. Desorption Force per Polystyrene Segment in Water. *Macromolecules* **2003**, *36*, 3779–3782.

(45) Prasath, S. S.; Brijitta, J.; Tata, B. V. R.; Joshi, R. G.; Chennakesavulu, K.; Gupta, D. K. Optical and rheological studies on weak gel-sol transition in aqueous

solutions of poly (N-isopropylacrylamide)-block-polystyrene. *eXPRESS Polymer Letters* **2017**, *11(7)*, 589–599.

(46) Hammouda, B. *Polymer Characteristics. Advances in Polymer Science*; Springer, Berlin, Heidelberg, 1993; Vol. 106.

(47) Buratti, E.; Tavagnacco, L.; Zanatta, M.; Chiessi, E.; Buoso, S.; Franco, S.; Ruzicka, B.; Angelini, R.; Orecchini, A.; Bertoldo, M.; Zaccarelli, E. The role of polymer structure on water confinement in poly(N-isopropylacrylamide) dispersions. *Journal of Molecular Liquids* **2022**, *355*, 118924.

(48) Michalska-Walkowiak, J.; Förster, B.; Hauschild, S.; Förster, S. Bistability, remanence, read/write-memory, and logic gate function via a stimuli-responsive polymer. *Adv. Mat.* **2022**, *34(13)*, 2108833.

(49) Lang, X.; Lenart, W.; Sun, J.; Hammouda, B.; Hore, M. J. A. Interaction and Conformation of Aqueous Poly(N-isopropylacrylamide) (PNIPAM) Star Polymers below the LCST. *Macromolecules* **2017**, *50(5)*, 2145–2154.

(50) Kawaguchi, T.; Kobayashi, K.; Osa, M.; Yoshizaki, T. Is a "Cloud-Point Curve" in Aqueous Poly(N-isopropylacrylamide) Solution Binodal? *J. Phys. Chem. B* **2009**, *113(16)*, 5440–5447.

(51) Hammouda, B. A new Guinier–Porod model. *J. Appl. Cryst.* **2010**, *43*, 716–719.

(52) Hammouda, B. Form Factors for Branched Polymers with Excluded Volume. *Journal of Research of the National Institute of Standards and Technology* **2016**, 139–164.

(53) Tsolou, G.; Stratikis, N.; Baig, C.; Stephanou, P. S.; Mavrantzas, V. G. Melt Structure and Dynamics of Unentangled Polyethylene Rings: Rouse Theory, Atomistic Molecular Dynamics Simulation, and Comparison with the Linear Analogues. *Macromolecules* **2010**, *43*, 10692–10713.

(54) Parekh, P.; Ohno, S.; Yusa, S.; Lage, E. V.; Casas, M.; Sández-Macho, I.; Aswal, V. K.; Bahadur, P. Surface and Aggregation Behavior of Pentablock Copolymer PNIPAM7-F127-PNIPAM7 in Aqueous Solutions. *The Journal of Physical Chemistry B* **2016**, *120*, 7569–7578, PMID: 27385006.

(55) Koga, T.; Tanaka, F.; Motokawa, R.; Koizumi, S.; M.Winnik, F. Theoretical modeling of associated structures in aqueous solutions of hydrophobically modified telechelic PNIPAM based on a neutron scattering study. *Macromolecules* **2008**, *41(23)*, 9413–9422.

(56) Cheng, R. R.; Hawk, A. T.; Makarov, D. E. Exploring the role of internal friction in the dynamics of unfolded proteins using simple polymer models. *J. Chem. Phys.* **2013**, *138*, 074112.

(57) Buvalaia, E.; Kruteva, M.; Hoffman, I.; Radulescu, A.; Förster, S.; Biehl, R. Interchain hydrodynamic interaction and internal friction of polyelectrolytes. *ACS Macro Lett.* **2023**, *12*, 1218–1223.

(58) Balacescu, L.; Schrader, T. E.; Radulescu, A.; Zolnierczuk, P.; Holderer, O.; Pasini, S.; Fitter, J.; Stadler, A. M. Transition between protein-like and polymer-like dynamic behavior: Internal friction in unfolded apomyoglobin depends on denaturing conditions. *Sci. Rep.* **2020**, *10*, 1570.

(59) Gonzalez-Burgos, M.; Asenjo-Sanz, I.; Pomposo, J. A.; Radulescu, A.; Ivanova, O.; Pasini, S.; Arbe, A.; Colmenero, J. Structure and Dynamics of Irreversible Single-Chain Nanoparticles in Dilute Solution. A Neutron Scattering Investigation. *Macromolecules* **2020**, *53(18)*, 8068–8082.

(60) Schulz, J. C. F.; Schmidt, L.; Best, R. B.; Dzubiella, J.; Netz, R. R. Peptide chain dynamics in light and heavy water: zooming in on internal friction. *J. Am. Chem. Soc.* **2012**, *134 (14)*, 6273–6279.

(61) Hayter, J.; Penfold, J. Self-consistent structural and dynamic study of concentrated micelle solutions. *J Chem Soc., Faraday Trans. 1* **1981**, *77*, 1851–1863.

(62) Richter, D.; Kruteva, M. Polymer dynamics under confinement. *Soft Matter* **2019**, *15*, 7316–7349.

(63) Glomann, T.; Hamm, A.; Allgaier, J.; Hübner, E. G.; Radulescu, A.; Farago, B.; Schneider, G. J. A microscopic view on the large scale chain dynamics in nanocomposites with attractive interactions. *Soft Matter* **2013**, *9*, 10559–10571.

(64) Poling-Skutvik, R.; Olafson, K. N.; Narayanan, S.; Stingaciu, L.; Faraone, A.; Conrad, J. C.; R, K. Confined dynamics of grafted polymer chains in solutions of linear polymer. *Macromolecules* **2017**, *50(18)*, 7372–7379.

(65) Krutyeva, M.; Wischnewski, A.; Monkenbusch, M.; Willner, L.; Maiz, J.; Mijangos, C.; Arbe, A.; Colmenero, J.; Radulescu, A.; Holderer, O.; Ohl, M.; Richter, D. Effect of nanoconfinement on polymer dynamics: Surface layers and interphases. *PRL* **2013**, *110*, 108303.

(66) Tavagnacco, L.; Zaccarelli, E.; Chiessi, E. On the molecular origin of the cooperative coil-to-globule transition of poly (N-isopropylacrylamide) in water. *Phys. Chem. Chem. Phys.* **2018**, *20*, 9997–10010.

(67) Fischer, J.; Radulescu, A.; Falus, P.; Richter, D.; Biehl, R. Structure and Dynamics of Ribonuclease A during Thermal Unfolding: The Failure of the Zimm Model. *The Journal of Physical Chemistry B* **2021**, *125*, 780–788, PMID: 33470118.

(68) Kanaya, T.; Monkenbusch, M.; Watanabe, H.; Nagao, M.; Richter, D. Dynamics of deuterated polystyrene-protonated butadiene diblock copolymer micelles by neutron spin echo. *J. Chem. Phys* **2005**, *122*, 144905.

(69) Zanatta, M.; Tavagnacco, L.; Buratti, E.; Chiessi, E.; Natali, F.; Bertoldo, M.; Orecchini, A.; Zaccarelli, E. Atomic scale investigation of the volume phase transition in concentrated PNIPAM microgels. *J. Chem. Phys.* **2020**, *152*, 204904.

(70) Volino, F.; Perrin, J.-C.; Lyonnard, S. Gaussian Model for Localized Translational Motion: Application to Incoherent Neutron Scattering. *The Journal of Physical Chemistry B* **2006**, *110*, 11217–11223.

(71) Monkenbusch, M.; Stadler, A.; Biehl, R.; Ollivier, J.; Zamponi, M.; Richter, D. Fast internal dynamics in alcohol dehydrogenase. *The Journal of Chemical Physics* **2015**, *143*, 075101.

(72) Hassani, A. N.; Haris, L.; Appel, M.; Seydel, T.; Stadler, A. M.; Kneller, G. R. Multiscale relaxation dynamics and diffusion of myelin basic protein in solution studied by quasielastic neutron scattering. *The Journal of Chemical Physics* **2022**, *156*, 025102.

(73) Ono, Y.; Shikata, T. Hydration and dynamic behavior of poly(N-isopropylacrylamide)s in aqueous solution: A sharp phase transition at the lower critical solution temperature. *Journal of the American Chemical Society* **2006**, *128*, 10030–10031.